Inorganic Chemistry

Article

pubs.acs.org/IC

Sr_2GaScO_5, $Sr_{10}Ga_6Sc_4O_{25}$, and $SrGa_{0.75}Sc_{0.25}O_{2.5}$: a Play in the Octahedra to Tetrahedra Ratio in Oxygen-Deficient Perovskites

Sergey V. Chernov,[†] Yuri A. Dobrovolsky,[†] Sergey Ya. Istomin,*[,‡] Evgeny V. Antipov,[‡] Jekabs Grins,[§] Gunnar Svensson,[§] Nadezhda V. Tarakina,[⊥,¶] Artem M. Abakumov,[¶] Gustaaf Van Tendeloo,[¶] Sten G. Eriksson,[∥] and Seikh M. H. Rahman[∥]

[†]Institute of Problems of Chemical Physics, RAS, Acad. Semenov avenue 1, 142432 Chernogolovka, Moscow Region, Russia

[‡]Department of Chemistry, Moscow State University, Leninskie Gory, 119991 Moscow, Russia

[§]Department of Materials and Environmental Chemistry, Stockholm University, S-10691 Stockholm, Sweden

[⊥]Physikalisches Institut, Universität Würzburg, Am Hubland, D-97074 Würzburg, Germany

[¶]EMAT, University of Antwerp, Groenenborgerlaan 171, B-2020 Antwerp, Belgium

[∥]Department of Chemical and Biological Engineering, Chalmers University of Technology, SE-412 96 Gothenburg, Sweden

Supporting Information

ABSTRACT: Three different perovskite-related phases were isolated in the $SrGa_{1-x}Sc_xO_{2.5}$ system: Sr_2GaScO_5, $Sr_{10}Ga_6Sc_4O_{25}$, and $SrGa_{0.75}Sc_{0.25}O_{2.5}$. Sr_2GaScO_5 (x = 0.5) crystallizes in a brownmillerite-type structure [space group (S.G.) *Icmm*, a = 5.91048(5) Å, b = 15.1594(1) Å, and c = 5.70926(4) Å] with complete ordering of Sc^{3+} and Ga^{3+} over octahedral and tetrahedral positions, respectively. The crystal structure of $Sr_{10}Ga_6Sc_4O_{25}$ (x = 0.4) was determined by the Monte Carlo method and refined using a combination of X-ray, neutron, and electron diffraction data [S.G. $I4_1/a$, a = 17.517(1) Å, c = 32.830(3) Å]. It represents a novel type of ordering of the B cations and oxygen vacancies in perovskites. The crystal structure of $Sr_{10}Ga_6Sc_4O_{25}$ can be described as a stacking of eight perovskite layers along the c axis ...[−(Sc/Ga)$O_{1.6}$−$SrO_{0.8}$−(Sc/Ga)$O_{1.8}$−$SrO_{0.8}$−]$_2$.... Similar to Sr_2GaScO_5, this structure features a complete ordering of the Sc^{3+} and Ga^{3+} cations over octahedral and tetrahedral positions, respectively, within each layer. A specific feature of the crystal structure of $Sr_{10}Ga_6Sc_4O_{25}$ is that one-third of the tetrahedra have one vertex not connected with other Sc/Ga cations. Further partial replacement of Sc^{3+} by Ga^{3+} leads to the formation of the cubic perovskite phase $SrGa_{0.75}Sc_{0.25}O_{2.5}$ (x = 0.25) with a = 3.9817(4) Å. This compound incorporates water molecules in the structure forming $SrGa_{0.75}Sc_{0.25}O_{2.5}\cdot xH_2O$ hydrate, which exhibits a proton conductivity of ~2.0×10^{-6} S/cm at 673 K.

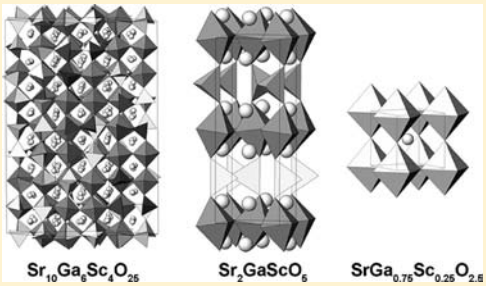

1. INTRODUCTION

Oxygen-deficient perovskites are known to have various important industrial applications, including high-temperature electrochemical devices, such as solid oxide fuel cells (SOFCs). In SOFCs, electrical energy is obtained through the conversion of chemical energy released in the redox reaction between the fuel, e.g., hydrogen (at the anode) and oxygen (at the cathode). Depending on the utilized type of ionic conductivity, SOFCs can be classified as proton or oxide-ion conductors. The former includes different high-temperature proton-conducting materials like doped cerium or zirconium perovskites ABO_3 (A = Sr, Ba; B = Ce, Zr) or oxygen-deficient perovskite-related niobium and tantalum oxides like $A_{6-2x}B_{2+2x}O_{11+3x}$ (A = alkaline-earth; B = Nb, Ta); see, for example, a recent review.[1] The latter includes various oxygen-deficient compounds, e.g., $Zr_{1-x}Y_xO_{2-x/2}$ (YSZ) and $La_{1-x}Sr_xGa_{1-y}Mg_yO_{3-z}$ (LSGM) with fluorite- and perovskite-related structures, respectively.

Among oxide-ion conductors with negligible electronic conductivity, complex oxides of the group 13 elements demonstrate the highest oxide-ion conductivity. This is related to a flexibility of the oxygen coordination environment for these elements, especially characteristic for the Ga^{3+} and In^{3+} cations. Thus, the oxide-ion conductivity of LSGM outperforms traditional SOFC materials like YSZ[2,3] and is considered as a base for the intermediate-temperature SOFC (IT-SOFC), operating at 500−700 °C. However, the use of LSGM in SOFCs is restricted by difficulties in obtaining single-phase material, the volatility of gallium at high temperatures, and its high reactivity toward metallic nickel, often used as a component of anodes in SOFCs. Another example is $Ba_2In_2O_5$ with the brownmillerite structure, which transforms at ~930 °C to the disordered perovskite with high oxide-ion conductivity.[4] The cubic perovskite phase can be stabilized by appropriate doping, and $Ba_{0.3}Sr_{0.2}La_{0.5}InO_{2.75}$ is known to exhibit oxide-ion conductivity up to 0.1 S/cm at 800 °C.[5]

Received: October 18, 2011
Published: December 22, 2011

dx.doi.org/10.1021/ic202236h | *Inorg. Chem.* 2012, 51, 1094−1103

Perovskite-like oxides $A^{2+}(B^{3+},B'^{3+})O_{2.5}$ (A = Sr, Ba; B = group 13 element; B′ = other trivalent cation with invariable oxidation state like Sc^{3+} or small rare-earth cations) are of interest as fast oxide-ion conductors used as electrolytes in SOFCs because they possess a high concentration of oxygen vacancies. In these oxides, the large B′ cation preferentially occupies octahedral positions, whereas the group 13 element has a coordination number of <6. Ba_2AlScO_5[6] and Ba_2GaScO_5[7] have ordered structures with hexagonal closed packing of the BaO_x layers (so-called anion-deficient hexagonal perovskites). In the $Sr(Sc,Al)O_{2.5}$ system, several compounds have been reported. $SrAl_{0.75}Sc_{0.25}O_{2.5}$ has a cubic structure [a = 7.9078(4) Å] with oxygen vacancies randomly distributed around two B cation sites.[8] Takeda et al.[9] have reported the formation of the cubic $SrAl_{0.5}Sc_{0.5}O_{2.5}$ perovskite with a = 3.9554(6) Å and the perovskite-related phases in the compositional range $SrAl_{0.5-x}Sc_{0.5+x}O_{2.5}$, where $0 \le x \le 0.15$. $SrAl_{0.5}Sc_{0.5}O_{2.5}$ exhibits a low oxide-ion conductivity of $\sim 10^{-4}$ S/cm at 1000 °C.

In the present paper, we report on the investigation of the $SrGa_{1-x}Sc_xO_{2.5}$ system, where three novel oxygen-deficient perovskites have been isolated: $SrGa_{0.75}Sc_{0.25}O_{2.5}$ with the cubic perovskite structure, brownmillerite-type Sr_2GaScO_5, and $Sr_{10}Ga_6Sc_4O_{25}$ with a novel type of ordering of the B cations and oxygen vacancies. The high-temperature conductivity of $SrGa_{0.75}Sc_{0.25}O_{2.5}$ in various atmospheres including wet gases was also studied.

2. EXPERIMENTAL SECTION

Samples of $SrGa_{1-x}Sc_xO_{2.5}$, where $0.05 \le x \le 0.75$, were prepared by polyacrylamide gel synthesis.[10] Stoichiometric mixtures of Sc_2O_3, Ga_2O_3, and $SrCO_3$ were dissolved in a minimal amount of concentrated HNO_3. Thereafter, an aqueous solution of ammonium citrate $(NH_3)_3$(cit) was added. The amount of citrate was calculated according to the chelate formula ML_n, where M is the metal, n its valence, and L a ligand (citric acid). Finally, the pH of the solution was adjusted to 7 by adding aqueous NH_3. Acrylamide and N',N'-methylendiacrylamide in quantities of 6 and 1 g/100 mL of solution, respectively, were dissolved separately in distilled water and mixed with the citrate solution. The resulting solution was heated to boiling, whereupon a few grains of α,α'-azoisobutyronitrile were added. The solution turned into a transparent colorless gel, which was placed into a furnace and slowly heated in air at a rate of 2 K/min up to 1173 K and then kept at this temperature for 2 h. The obtained powder was grinded, pressed into pellets, and heated at 1473−1673 K for 15−24 h.

For the preparation of the zirconium-doped samples $SrGa_{0.5}Sc_{0.5-x}Zr_xO_{2.5+x/2}$, where x = 0.01−0.12 and Δx = 0.01, stoichiometric mixtures of Sc_2O_3 and Ga_2O_3 were dissolved in a minimal quantity of concentrated nitric acid. The obtained solution, together with stoichiometric amounts of $SrCO_3$ and $ZrO(NO_3)_2 \cdot 5.3H_2O$, was added into the melt of citric acid and heated on a hot plate in air to achieve the formation of a brown viscous mass. Further annealing was performed at 873 K for 2 h. The obtained powder was grinded, pressed in pellets, and finally heated in air at 1673 K for 15 h.

The phase purity of the compounds was checked by powder X-ray diffraction (PXRD) recorded with a Huber G670 Guinier diffractometer (Cu Kα_1 radiation, image foil detector). High-temperature PXRD data for $SrGa_{0.75}Sc_{0.25}O_{2.5}$ and room-temperature data for the Rietveld refinement of the Sr_2GaScO_5 crystal structure were collected in air using a Bruker D8-Advance diffractometer (Cu Kα_1 radiation, Vantec PSD) in reflection mode equipped with a high-temperature camera XRK-900 (Anton Paar). The PXRD pattern for the structural refinement of the $Sr_{10}Ga_6Sc_4O_{25}$ crystal structure was collected with a PANalytical X'pert PRO MPD diffractometer using Cu Kα_1 radiation, variable slits with a constant area of 4 cm^2 irradiated, and a step size of 0.0167°, in the 2θ range 5−125° and with a total measurement time of 30 min, yielding patterns with maximum peak intensities of ca. 50 000 counts. The patterns were converted to corresponding 0.5° fixed-slit data using the PANalytical X'Pert HighScore Plus software. Neutron powder diffraction (NPD) data were collected on the GEM diffractometer at the spallation source ISIS, Rutherford Appleton Laboratory, U.K. Rietveld structure refinements were made with the *GSAS* program package.[11]

Electron diffraction (ED) patterns were recorded with JEOL JEM2000FX and Philips CM20 transmission electron micrographs with a LaB_6 filament, equipped with a double tilt sample holder ±45°, operating at 200 kV. The sample was fixed on a copper grid with holey carbon by dipping the grid through an ethanol suspension of the sample.

Electrical conductivity measurements were performed by alternating-current impedance spectroscopy using a Solartron 1260 frequency response analyzer in the frequency range of 1 Hz to 1 MHz for $SrGa_{0.75}Sc_{0.25}O_{2.5}$. For the electrical conductivity measurements, pellets of $SrGa_{0.75}Sc_{0.25}O_{2.5}$ (d = 12.4 mm; h = 1.5 mm) were coated by platinum paste (Heraeus CL 11-5100) and heated at 1273 K for 1 h.

A Netzsch DIL 402C dilatometer operated in air (298−1173 K, 10 K/min) was used for thermal expansion coefficient measurements of the Sr_2GaScO_5 sample. For thermal expansion measurements, oxide powder was pressed into pellets of 8 mm diameter and 5−5.5 mm height and annealed at 1473 K.

Thermogravimetric analysis (TGA) studies were carried out in argon (Linde Gas, 99.997%, 5 ppm H_2O) or nitrogen (AGA, 5 ppm H_2O) with gas flow rates of 20 mL/min from 298 to 1273 K at a heating rate of 5 or 15 K/min using a Netzsch STA 409 PC.

3. RESULTS

Three novel compounds with different perovskite-related structures were found in the $SrGa_{1-x}Sc_xO_{2.5}$ system. The formation of single-phase samples was observed for the compositions $SrGa_{1-x}Sc_xO_{2.5}$, where x = 0.25, 0.375, and 0.5. The color of the samples was crème-brown for x = 0.25 and white for x = 0.375 and 0.5. The samples with $x \le 0.25$ contained a significant amount of $Sr_3Ga_4O_9$, while for $0.25 < x < 0.35$, an unidentified admixture phase(s) was observed as well. The $0.375 < x < 0.5$ samples contained a mixture of the two phases with x = 0.375 and 0.5. Also, the samples with $0.5 < x \le 0.75$ were not single phase and contained unknown admixture phase(s), together with the x = 0.5 phase.

3.1. Sr_2GaScO_5 with the Brownmillerite Structure. Single-phase samples of $SrGa_{0.5}Sc_{0.5}O_{2.5}$ were obtained by annealing at 1473 K for 15 h followed by cooling to room temperature with a rate of ∼150 K/h. The PXRD pattern of $SrGa_{0.5}Sc_{0.5}O_{2.5}$ was indexed with an orthorhombic unit cell with a = 5.91048(5) Å, b = 15.1594(1) Å, and c = 5.70926(4) Å, suggesting the formation of the brownmillerite-type structure, hereinafter referred to as Sr_2GaScO_5. The $h + k + l = 2n$ reflection condition unambiguously suggests a body-centered orthorhombic unit cell. It is well-known that, depending on the relative orientation of the tetrahedral chains between the octahedral layers in brownmillerite, two highly ordered structures having space groups *Ibm*2 (No. 46) and *Pcmn* (No. 62) can be obtained. A random ordering of the tetrahedral layers leads to space group *Icmm* (No. 74).

Reflection conditions do not allow one to distinguish between *Ibm*2 and *Icmm* space groups. The Sr_2GaScO_5 structure was refined in both space groups using PXRD data. In both models, we observed complete ordering of the B cations over two sites in the brownmillerite structure, where the large Sc^{3+} occupies the octahedral position and Ga^{3+} is situated in the tetrahedral one. Refinement in *Icmm* led to slightly better R values (R_{wp} = 0.0796, R_p = 0.0618, and χ^2 = 2.23) compared to *Ibm*2 (R_{wp} = 0.0804, R_p = 0.0623, and χ^2 = 2.28). Moreover, some interatomic distances between B cations and O atoms in *Ibm*2 were unreasonably short. For example, two distances

dx.doi.org/10.1021/ic202236h | *Inorg. Chem.* 2012, 51, 1094−1103

Table 1. Summary of the Results of the Least-Square Fits, Final Atomic Coordinates, and Displacement Parameters for Sr_2GaScO_5

space group	*Icmm*
a, Å	5.91159(7)
b, Å	15.1526(2)
c, Å	5.70458(7)
Z	8
cell volume, Å^3	510.99(2)
calcd density, g/cm^3	4.808
radiation	Cu Kα_1, λ = 1.54060 Å
2θ range; step, deg	$5 \le 2\theta \le 100$, 0.0081
params refined	37
χ^2, R_F^2, R_{wp}, R_P	2.23; 0.0406, 0.0796, 0.0618

atom	site	*x*	*y*	*z*	$U_{iso} \times 100$/Å^2	occupancy
Sr	8h	0.0200(1)	0.11199(4)	0.5	1.09(9)	1
Sc	4a	0	0	0	0.9(1)	1
Ga	8i	−0.0718(2)	0.25	−0.0268(7)	1.3(1)	0.5
O1	8g	0.25	−0.0140(2)	0.25	0.4(1)	1
O2	8h	0.0719(6)	0.1458(3)	0	2.2(2)	1
O3	8i	0.833(1)	0.25	0.660(1)	2.0	0.5

between Sc and equatorial O atoms were 1.92(1) Å in comparison with a typical Sc−O distance of ∼2.1 Å. This indicates that the correct space group for Sr_2GaScO_5 is *Icmm*. The final refined atomic parameters are given in Table 1; the main interatomic distances are given in Table 2. Experimental,

Table 2. Selected Interatomic Distances (Å) for Sr_2GaScO_5

O1−Sc	(×4)	2.0647(4)
O2−Sc	(×2)	2.250(4)
O2−Ga	(×2)	1.799(4)
O3−Ga	(×2)	1.877(8)
Sr−O1	(×2)	2.605(2)
	(×2)	2.743(3)
Sr−O2		2.466(4)
	(×2)	2.9142(7)
Sr−O3	(×2)	2.534(4)

calculated, and difference diffraction profiles are shown in Figure 1. As mentioned above, in the crystal structure of Sr_2GaScO_5,

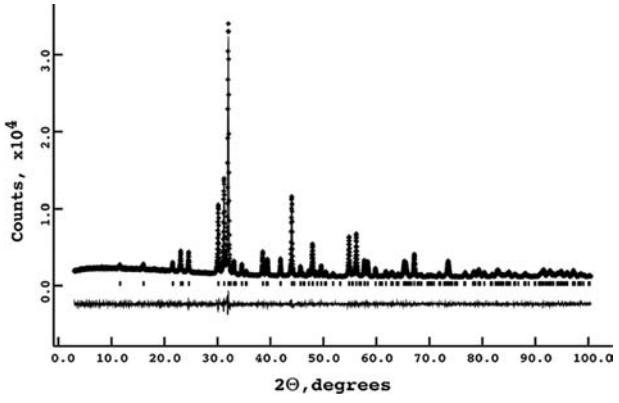

Figure 1. Observed, calculated, and difference between them PXRD profiles for Sr_2GaScO_5.

there is a full order of Sc^{3+} and Ga^{3+} cations over octahedral and tetrahedral positions, respectively. The scandium octahedron is rather distorted with substantially elongated Sc−O axial bonds [2.250(4) Å] in comparison with equatorial ones [2.0647(4) Å]. This, together with disorder in the tetrahedral layers, leads to distortion of the gallium tetrahedron, with the Ga−O bond length varying between 1.799(4) and 1.877(8) Å.

The differential scanning calorimetry experiment on Sr_2GaScO_5 shows a strong exothermal effect at ∼1663 K, which can be most likely interpreted as melting. The PXRD pattern of the Sr_2GaScO_5 sample quenched from 1723 K (Figure 2) can be indexed in a cubic perovskite cell with

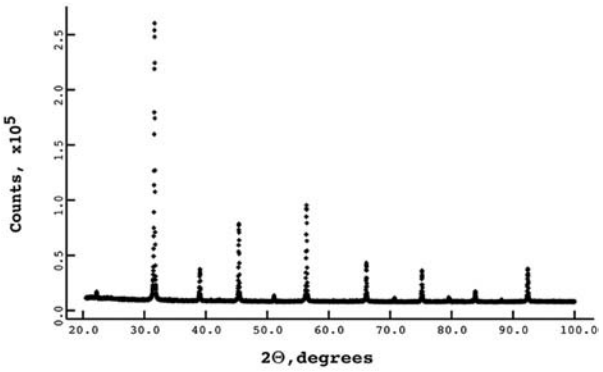

Figure 2. PXRD pattern of the Sr_2GaScO_5 sample quenched from 1723 K.

a = 3.99382(1) Å because no additional reflections indicating either superstructure or splitting of the perovskite subcell reflections are observed. However, one cannot exclude the brownmillerite-like ordering of the B cations and oxygen vacancies on the level of the microdomains[12] in this metastable phase.

In order to stabilize a disordered cubic perovskite, heterovalent substitution of Sc^{3+} by Zr^{4+} according to the formula $SrGa_{0.5}Sc_{0.5-x}Zr_xO_{2.5+x/2}$, where Δx = 0.01, was performed. The samples were annealed at 1673 K and cooled to room temperature at the rate of 150 K/h. A solid solution with a cubic perovskite structure was formed in a narrow composition range of x = 0.03−0.1. For the samples with x = 0.01 and 0.02 Sr_2GaScO_5 and the cubic perovskite phase were observed, whereas for the samples with $x > 0.1$, admixtures of $SrZrO_3$ and Sc_2O_3 were found. The compositional dependence of the unit cell parameter of $SrGa_{0.5}Sc_{0.5-x}Zr_xO_{2.5+x/2}$ is shown in Figure 3.

dx.doi.org/10.1021/ic202236h | *Inorg. Chem.* 2012, 51, 1094−1103

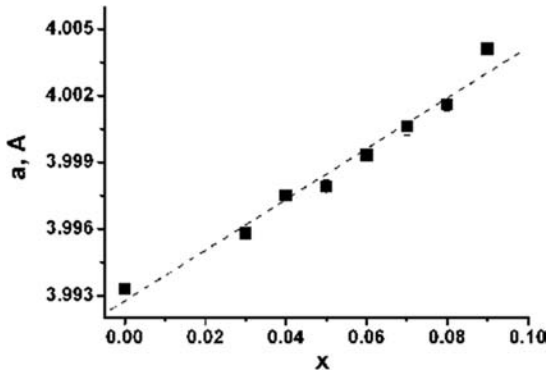

Figure 3. Compositional dependence of the unit cell parameters for $SrGa_{0.5}Sc_{0.5-x}Zr_xO_{2.5+x/2}$.

The minor increase of the unit cell parameter of the perovskite phase with the zirconium content is most probably associated with an increase of the oxygen content because the ionic radius of Zr^{4+} (r = 0.84 Å) is slightly smaller than that of Sc^{3+} (r = 0.87 Å [13]).

3.2. Novel Oxygen-Deficient Perovskite $Sr_{10}Ga_6Sc_4O_{25}$. The $SrGa_{0.625}Sc_{0.375}O_{2.5}$ sample was prepared by annealing in air at 1473 K for 15 h. The PXRD pattern suggests the formation of a perovskite-related phase. However, in addition to the perovskite subcell reflections, there were numerous weak superstructure reflections, which required selected-area ED (SAED) to identify the supercell. The SAED investigation revealed the material to be well crystallized without indications of disorder. A number of tilt series were recorded, and the relationship between the supercell and perovskite subcell was found to be $a^* = 1/10(2a^*_p - b^*_p)$, $b^* = 1/10(-a^*_p + 2b^*_p)$, and $c^* = 1/8c^*_p$. The superstructure reflections can thus be indexed with a tetragonal unit cell, $a = b \approx 2\sqrt{5}a_p \approx 17.5$ Å and $c \approx 8a_p \approx 33$ Å, with $a_p \approx 4$ Å (subcell parameter). A number of SAED patterns corresponding to low-index zone axes in the perovskite subcell in addition to low-index zone axes in the supercell are shown in Figure 4.

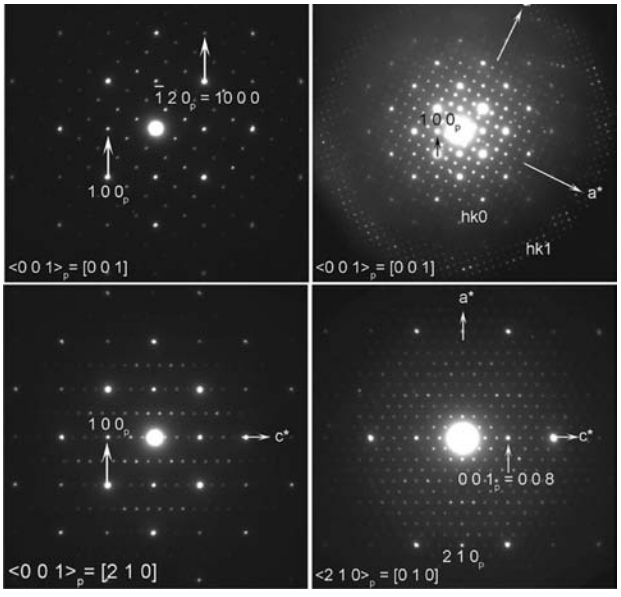

Figure 4. SAED patterns of $Sr_{10}Ga_6Sc_4O_{25}$. Selected low-index zone axes patterns in the perovskite subcell are shown as well in the supercell. The relationship between the perovskite subcell and supercell is $a = b \approx 2\sqrt{5}a_p$ and $c \approx 8a_p$.

SAED indicates the reflection conditions hkl ($h + k + l = 2n$), $hk0$ (h, $k = 2n$), and $00l$ ($l = 4n$), consistent with the space group $I4_1/a$ (No. 88). In the Rietveld refinement of the crystal structure (see below), we have found that the composition of the phase corresponds to the formula $Sr_{10}Ga_6Sc_4O_{25}$, which differs only slightly from the composition of the sample $SrGa_{0.625}Sc_{0.375}O_{2.5}$. Therefore, the composition of the phase will hereinafter be referred to as $Sr_{10}Ga_6Sc_4O_{25}$.

3.2.1. Refinement of the Crystal Structure of $Sr_{10}Ga_6Sc_4O_{25}$. The PXRD pattern of $Sr_{10}Ga_6Sc_4O_{25}$ was fully indexed with the unit cell parameters and space group obtained from the SAED study [a = 17.517(1) Å; c = 32.830(3) Å]. The structure was solved using the direct space Monte Carlo simulation program *FOX*[14] applied to PXRD data. The multiplicity for a general site in the space group $I4_1/a$ is 16, and it was assumed that the unit cell contains 16 formula units of $Sr_{10}Ga_6Sc_4O_{25}$. The solution of the structure was simplified by the fact that it contains B cations with different crystal chemistry. Large Sc^{3+} cations are known to possess octahedral oxygen coordination. A localization of all four ScO_6 octahedra and all Sr atoms in the structure, accounting for ca. 80% of the total scattering power, would, in the case of an ordered structure, probably enable the remaining atoms to be located subsequently. Structure optimization was accordingly carried out using *FOX*, with 10 Sr atoms at general 16f positions and four ScO_6 semirigid octahedra introduced randomly and using the dynamical occupancy correction. Four Sr atoms were found to occupy special 8e positions, and eight were located at 16f positions. After the Sr atoms were located, six Ga atoms were randomly introduced in 16f positions. Probable Sc/Ga atom positions could at this stage also be inferred from the partial structure model. The difficulty in assigning the Sc and Ga atoms to different positions was overcome during a considerably long optimization. Several O atoms of the ScO_6 octahedra atoms were located by first refining the structure model using the full PXRD data range. The obtained refined atom positions were then fixed, and *FOX* was used to find the positions of the missing atoms.

The final refinement was performed in the *GSAS* program package using simultaneously both the PXRD data and time-of-flight NPD data. In total, 310 variables were refined. Final reliability factors were χ^2_{tot} = 3.56 and R_F^2 = 0.023 for the PXRD data (4475 reflections) and R_F^2 = 0.0339 for the NPD data (154.4° data bank, 7074 reflections at 1.77 < d < 0.75 Å; see Table 3). Observed, calculated, and difference PXRD and NPD profiles are given in Figure 5a,b. Final atomic coordinates and displacement parameters are given in Table 1 in the Supporting Information and selected bond distances in Table 4. The variations in the bond lengths are 1.97−2.28 Å (average distance 2.105 Å) for the ScO_6 octahedra and 1.76−1.93 Å (average distance 1.831 Å) for the GaO_4 tetrahedra. These values are within the ranges typical for the Sc−O and Ga−O bond lengths observed in other oxides.

The crystal structure of $Sr_{10}Ga_6Sc_4O_{25}$ (Figure 6) represents the novel type of ordering of the B cations and oxygen vacancies in perovskites. It can be described as a sequence of eight perovskite layers along to the c axis. There are only two unique $(Sc/Ga)O_x$ layers in the structure, named layers 1 (Figure 7a) and 2 (Figure 7b). Other layers are related to them by the symmetry elements of the $I4_1/a$ space group. As in the structure of brownmillerite Sr_2GaScO_5, Ga and Sc cations are fully ordered in the structure, with Ga^{3+} and Sc^{3+} located in tetrahedra and octahedra, respectively. However, in comparison

dx.doi.org/10.1021/ic202236h | Inorg. Chem. 2012, 51, 1094−1103

Table 3. Summary of the Results of the Least-Squares Fits to the PXRD (NPD) Data Collected for $Sr_{10}Ga_6Sc_4O_{25}$

space group	$I4_1/c$
a, Å	17.52963(4)
c, Å	32.85749(9)
Z	16
cell volume, Å^3	10096.71(6)
calcd density, g/cm^3	4.932
PXRD data set:	
radiation	Cu Kα_1, λ = 1.54060 Å
2θ range; step, deg	$5 \le 2\theta \le 125$, 0.0167
R_F^2, R_{wp}, R_p	0.023, 0.0374, 0.0294
NPD data set:	
d range, Å	0.75−14
R_F^2, R_{wp}, R_p	0.0339, 0.0273, 0.0231
params refined	310
χ_{tot}^2	3.56

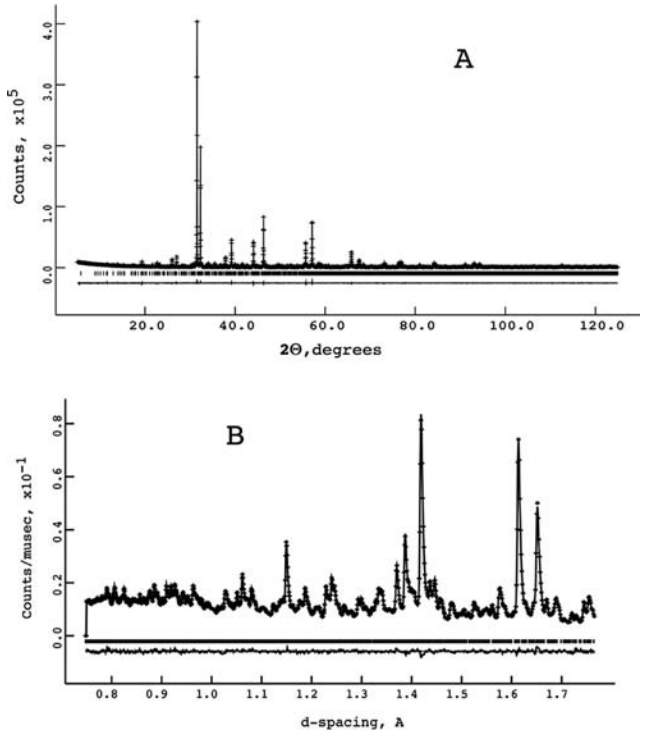

Figure 5. Observed, calculated, and difference between them PXRD (a) and NPD (b) profiles for $Sr_{10}Ga_6Sc_4O_{25}$.

with the brownmillerite, gallium tetrahedra and scandium octahedra are present in all layers. Each layer consists of 12 GaO_4 tetrahedra and 8 ScO_6 octahedra. The arrangement of the scandium octahedra in layers 1 and 2 is different. In layer 1, there are units of four corner-sharing ScO_6 octahedra, while in layer 2, only pairs of corner-sharing ScO_6 octahedra are present. These units are connected through the GaO_4 tetrahedra. There are two tetrahedral groups marked in green and yellow in Figure 7a,b. The first group (yellow in Figure 7) represents a pair of tetrahedra with a common corner. They are connected with a pair of ScO_6 octahedra. Such an arrangement is also observed between octahedra and tetrahedra along the direction of tetrahedral chains in the neighboring layers of the brownmillerite structure. In the second group (green in Figure 7), namely, $Ga2O_4$ in layer 1 and $Ga5O_4$ in layer 2, one of the tetrahedral vertexes (O6 and O15, respectively) is not connected to other Ga/Sc polyhedra. In layer 1, the remaining O atoms of the $Ga2O_4$ tetrahedra are connected with both tetrahedral and octahedral units, while in layer 2, the $Ga5O_4$ tetrahedra are connected with the octahedral units only. This leads to different orientations of the $Ga2O_4$ and $Ga5O_4$ tetrahedra [O15 belongs to the $(Sc/Ga)O_x$ layer, while O6 belongs to the SrO_y layer]. As a result, the oxygen content of layer 1 is $(Sc/Ga)O_{1.6}$, while it is $(Sc/Ga)O_{1.8}$ for layer 2. Therefore, the sequence of layers along to the c axis can be written as ...$[-(Sc/Ga)O_{1.6}-SrO_{0.8}-(Sc/Ga)O_{1.8}-SrO_{0.8}-]_2$....

3.3. $SrGa_{0.75}Sc_{0.25}O_{2.5}$ with a Cubic Perovskite Structure. The PXRD pattern of the sample with the nominal composition $SrGa_{0.75}Sc_{0.25}O_{2.5}$ (Figure 8) was indexed with a cubic perovskite cell with the unit cell parameter a = 3.9817(4) Å. The presence of weak (<%1) reflections from $Sr_3Ga_4O_9$[15] and unidentified phases was observed in the PXRD pattern. All attempts to prepare a single-phase sample by slightly varying the cation content off the stoichiometric $SrGa_{0.75}Sc_{0.25}O_{2.5}$ composition were unsuccessful. Thorough analysis of the profiles of the reflections at the PXRD pattern did not indicate deviation from the cubic symmetry. The primitive cubic unit cell was also supported by the absence of superstructure reflections in the SAED patterns of $SrGa_{0.75}Sc_{0.25}O_{2.5}$ (Figure 9a). The B cations as well as oxygen vacancies thus do not exhibit long-range order, although there is short-range order forming domains as seen in diffuse scattering in the [001] and [1−30] SAED patterns and in a corresponding a dark-field image from diffuse scattering of the former (Figure 9b).

In order to determine the thermal expansion properties of $SrGa_{0.75}Sc_{0.25}O_{2.5}$, a high-temperature PXRD study was performed. Temperature variation of the unit cell parameter is shown in Figure 10. Two regions with different thermal expansion coefficients (TECs) are observed. In the low-temperature region (298−498 K), the TEC value is 16.1 ppm/K, while it decreases sharply to 11.8 ppm/K in the high-temperature region (698−1098 K). The latter value is close to 11.2 ppm/K obtained from dilatometry data for the Sr_2GaScO_5 brownmillerite.

Combined thermal analysis and mass spectrometry studies revealed the release of water from the $SrGa_{0.75}Sc_{0.25}O_{2.5}$ sample in the temperature range of 500−673 K. The measured weight loss corresponds to the composition $SrGa_{0.75}Sc_{0.25}O_{2.5}\cdot 0.13H_2O$. The unit cell parameter of $SrGa_{0.75}Sc_{0.25}O_{2.5}\cdot xH_2O$ increases with increasing water content (x). For example, the unit cell parameter of the $SrGa_{0.75}Sc_{0.25}O_{2.5}$ sample treated in moisturized N_2 at 488 K for 3 days [a = 3.989(1) Å] is substantially larger compared to that for the sample annealed in dry argon at 1173 K for 1 h [a = 3.973(1) Å]. This explains the existence of two regions with different TEC values shown in Figure 10. The absorption of water by $SrGa_{0.75}Sc_{0.25}O_{2.5}$ seems to be the first step of the decomposition of the compound in wet air. Holding $SrGa_{0.75}Sc_{0.25}O_{2.5}$ at 343 K for 2 days in air saturated with water vapor leads to the complete decomposition of the compound. Only reflections from $SrCO_3$ are observed on the PXRD pattern, indicating the formation of amorphous products containing scandium and gallium. The decomposition seems to be accelerated by the formation of the thermodynamically stable $SrCO_3$ due to a reaction between $SrGa_{0.75}Sc_{0.25}O_{2.5}\cdot xH_2O$ and CO_2 present in air. However, the decomposition process is rather slow at room temperature in air with natural humidity, and $SrGa_{0.75}Sc_{0.25}O_{2.5}$ samples can thus be stored in these conditions for a prolonged period of time.

dx.doi.org/10.1021/ic202236h | Inorg. Chem. 2012, 51, 1094−1103

Table 4. Selected Bond Lengths for the Crystal Structure of $Sr_{10}Ga_6Sc_4O_{25}$

Sc1	O8	2.19(1)		Sc2	O9	2.28(1)	Sc3	O1	2.22(1)		Sc4	O4	2.17(1)
	O10	2.14(1)			O12	2.07(1)		O5	2.16(1)			O17	2.04(1)
	O16	2.02(1)			O13	2.13(1)		O14	2.10(1)			O20	2.13(1)
	O18	2.04(1)			O19	2.17(1)		O22	1.97(1)			O21	2.12(1)
	O21	2.04(1)			O22	2.13(1)		O24	2.07(1)			O25	2.11(1)
	O23	2.05(1)			O23	2.10(1)		O24	2.01(1)			O25	2.08(1)
Ga1	O1	1.81(1)		Ga2	O5	1.81(1)	Ga3	O2	1.88(1)		Ga4	O11	1.87(1)
	O2	1.79(1)			O6	1.80(1)		O9	1.85(1)			O12	1.89(1)
	O3	1.86(1)			O7	1.93(1)		O10	1.81(1)			O13	1.81(1)
	O4	1.77(1)			O8	1.81(1)		O11	1.84(1)			O14	1.86(1)
Ga5	O15	1.79(1)		Ga6	O3	1.83(1)							
	O16	1.85(1)			O7	1.76(1)							
	O17	1.83(1)			O19	1.83(1)							
	O18	1.84(1)			O20	1.82(1)							
Sr1	O17	2.95(1)	(×2)	Sr2	O1	2.773(7)	Sr3	O4	2.49(1)		Sr4	O2	2.767(9)
	O18	2.799(9)	(×2)		O2	2.88(1)		O8	2.62(1)			O3	2.86(1)
	O21	3.122(7)	(×2)		O5	2.833(9)		O10	2.66(1)			O5	2.81(1)
	O25	2.82(1)	(×2)		O6	2.923(8)		O15	3.07(1)			O7	3.02(1)
	O25	2.64(1)	(×2)		O11	2.551(9)		O16	2.53(1)			O8	3.15(1)
					O13	3.10(1)		O17	2.60(1)			O9	2.837(9)
					O14	2.57(1)		O20	2.65(1)			O15	2.51(1)
					O22	2.507(8)						O18	2.872(9)
					O24	2.782(9)						O22	2.81(1)
												O23	2.60(1)
Sr5	O7	2.51(1)	(×2)	Sr6	O1	2.479(7)	Sr7	O6	2.640(9)		Sr8	O1	2.883(8)
	O8	2.74(1)	(×2)		O5	2.84(1)		O7	3.13(1)	(×2)		O3	2.70(1)
	O16	2.73(1)	(×2)		O8	2.76(1)		O12	2.73(1)	(×2)		O5	2.64(1)
	O18	2.554(9)	(×2)		O10	2.63(1)		O13	2.995(9)	(×2)		O9	2.62(1)
					O12	2.80(1)		O19	2.65(1)	(×2)		O11	2.952(9)
					O14	3.07(1)						O13	2.428(9)
					O22	2.937(8)						O14	2.50(1)
					O23	2.52(1)						O19	2.79(1)
					O24	2.51(1)						O19	2.79(1)
Sr9	O2	2.88(1)		Sr10	O3	3.05(1)	Sr11	O12	2.71(1)	(×2)	Sr12	O2	2.90(1)
	O3	2.87(1)			O4	2.85(1)		O14	3.004(9) (x2)			O6	2.412(8)
	O4	3.15(1)			O9	2.476(9)		O22	2.98(1)	(×2)		O10	3.04(1)
	O10	3.36(1)			O17	2.84(1)		O24	2.604(9)	(×2)		O11	2.803(9)
	O15	2.35(1)			O18	2.736(9)		O24	2.89(1)	(×2)		O12	2.95(1)
	O16	2.78(1)			O19	2.91(1)						O19	2.60(1)
	O17	2.70(1)			O21	2.812(8)						O21	2.83(1)
	O20	2.88(1)			O25	2.61(1)						O21	2.554(8)
	O21	2.527(8)										O23	2.87(1)
	O25	2.70(1)											

3.3.1. Study of the Proton Conductivity in $SrGa_{0.75}Sc_{0.25}O_{2.5}$. Because scandium-containing perovskites, like doped $LaScO_3$, are known to exhibit high-temperature proton conductivity,[16−18] we have studied the high-temperature conductivity of $SrGa_{0.75}Sc_{0.25}O_{2.5}$. A water-saturated sample of $SrGa_{0.75}Sc_{0.25}O_{2.5}$ was prepared by heating the as-prepared samples at 488 K for 3 days in a flow of N_2 saturated with water vapor at 363 K, p_{H_2O} = 0.69 atm (so-called prehydrated samples). The study of the sample by TGA in dry N_2 at 298−1273 K (Figure 1 in the Supporting Information) shows that starting from ∼500 K it exhibits significant mass loss due to the release of water molecules from the crystal structure. The weight of the sample stabilizes at ∼1150 K. The composition of the prehydrated sample was calculated from TGA data as $SrGa_{0,75}Sc_{0,25}O_{2,5}\cdot 0.043H_2O$. No mass gain was observed in the cooling cycle.

Conductivity measurements were performed on the prehydrated samples in the following cycle: (1) the prehydrated samples were heated to 1273 K in dry argon; (2) thereupon, the samples were cooled to 423 K in dry argon; (3) finally, the samples were heated to 1273 K in wet argon and the conductivity was measured in the cooling cycle.

Complex impedance plots for prehydrated $SrGa_{0.75}Sc_{0.25}O_{2.5}$ samples in heating and cooling cycles in dry argon are presented in Figure 2 in the Supporting Information with the equivalent circuit model used for analysis of the impedance data shown on the inset. At temperatures higher than 773 K, it was difficult to separate bulk and grain boundary conductivities; therefore, only the values of the total conductivities are presented.

The corresponding Arrhenius plots are shown in Figure 11, from which it is clear that the total conductivity of the prehydrated samples is higher in the heating cycle than in the cooling cycle in dry argon, especially at T < 773 K. Therefore, one can conclude that within this temperature range the proton conductivity dominates because of the presence of water

dx.doi.org/10.1021/ic202236h | Inorg. Chem. 2012, 51, 1094−1103

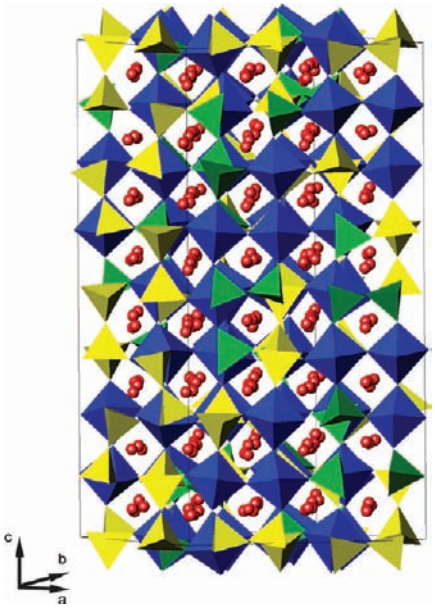

Figure 6. Crystal structure of $Sr_{10}Ga_6Sc_4O_{25}$. Red spheres are Sr^{2+} cations; Sc^{3+} cations are located in octahedra (blue) and Ga^{3+} cations in tetrahedra (yellow and green).

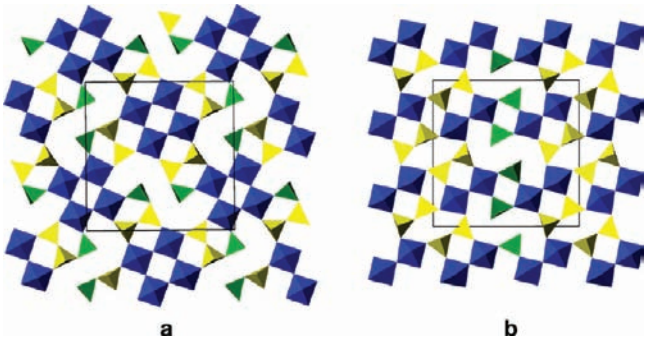

Figure 7. Two unique $(Sr/Ga)O_x$ layers in the crystal structure of $Sr_{10}Ga_6Sc_4O_{25}$ with different oxygen contents: $(Sc/Ga)O_{1.6}$, layer 1 (a); $(Sc/Ga)O_{1.8}$, layer 2 (b). GaO_4 tetrahedra belong to two groups with all vertexes shared with other Sc/Ga polyhedra (marked green) or with some O atoms not connected to other Sc/Ga polyhedra (marked yellow).

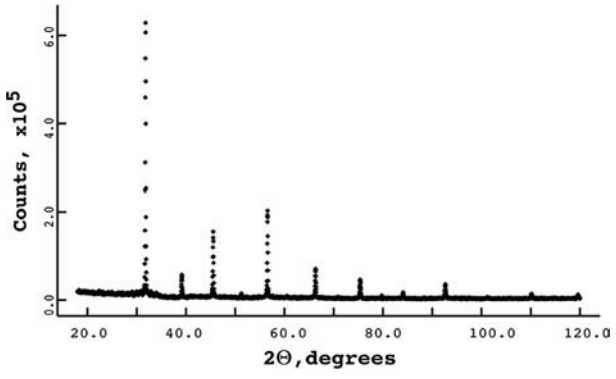

Figure 8. PXRD pattern of the $SrGa_{0.75}Sc_{0.25}O_{2.5}$ sample.

molecules in the crystal structure. This idea is supported by the fact that the water-free samples obtained after the heating cycle in dry argon show much higher conductivity at $T < 773$ K in wet argon in comparison with dry argon (compare curves 2 and 3 in Figure 11).

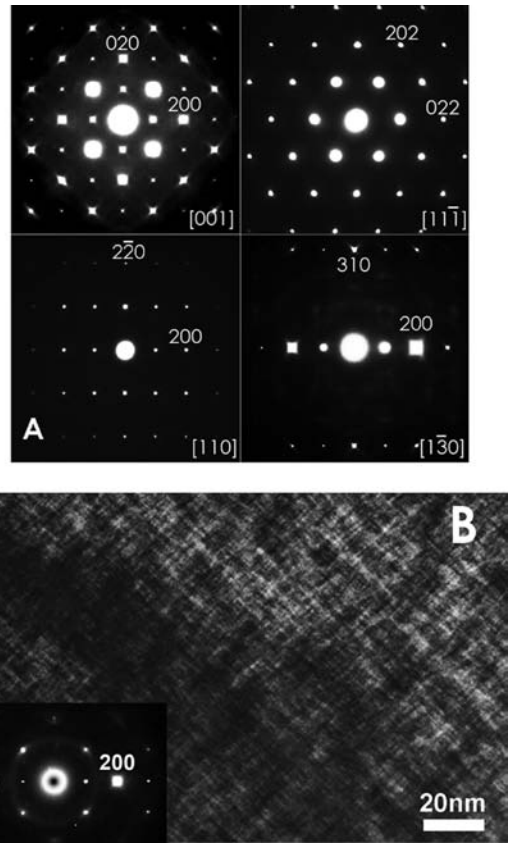

Figure 9. (a) SAED patterns of the cubic perovskite $SrGa_{0.75}Sc_{0.25}O_{2.5}$ viewed along [001], [11−1], [110], and [1−30]. (b) Dark-field image from the diffuse intensities in the [001] SAED pattern.

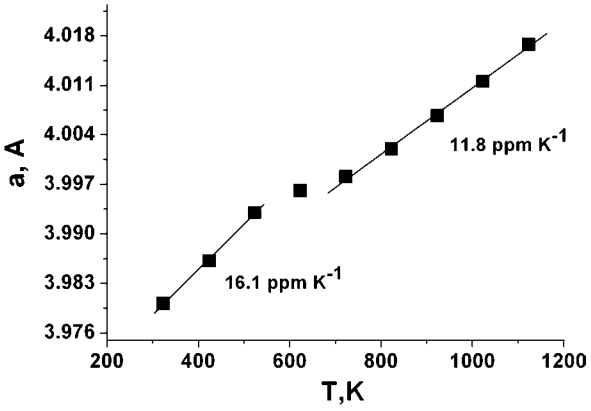

Figure 10. Temperature variation of the unit cell parameter of $SrGa_{0.75}Sc_{0.25}O_{2.5}$ determined from high-temperature PXRD data. TECs for different temperature ranges are given.

Assuming that proton conduction has no effect on other charge carrier contributions, the pure protonic conductivity σ_H can be calculated as the difference between the conductivity in H_2O-saturated argon, σ_{wet}, and the conductivity of the water-free sample obtained during the cooling cycle in dry argon, σ_{dry}:[19]

$$\sigma_H = \sigma_{wet} - \sigma_{dry}$$

The corresponding Arrhenius plot for pure protonic conductivity is shown in Figure 12.

dx.doi.org/10.1021/ic202236h | *Inorg. Chem.* 2012, 51, 1094−1103

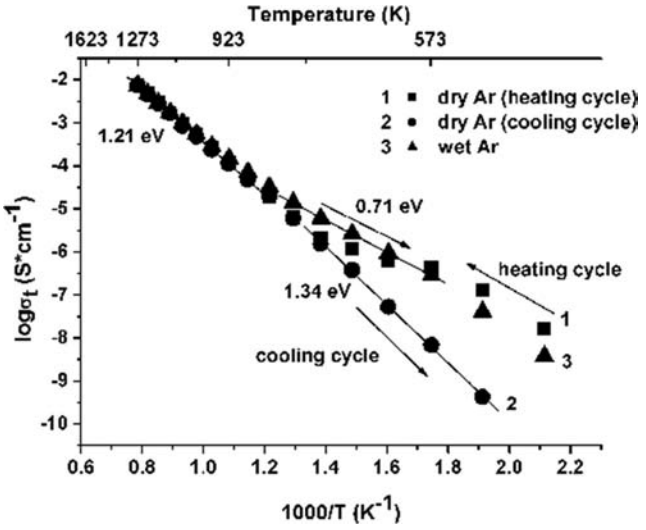

Figure 11. Temperature dependences (Arrhenius plots) of the total conductivities of the prehydrated $SrGa_{0.75}Sc_{0.25}O_{2.5}$ samples in heating and cooling cycles in dry argon. Curve 1 corresponds to the heating of the prehydrated sample in dry argon; curve 2 corresponds to the cooling of the water-free sample in dry argon; curve 3 corresponds to the heating of the water-free sample in wet argon.

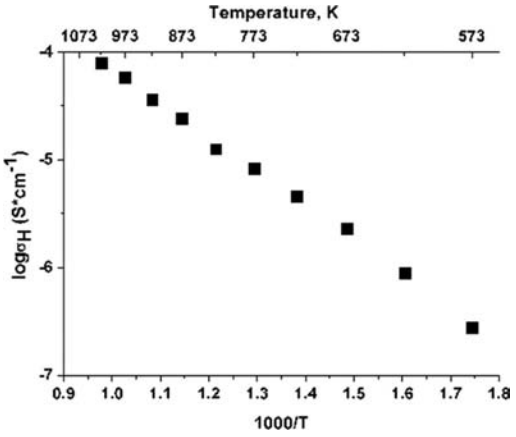

Figure 12. Temperature dependence (Arrhenius plot) of the proton conductivity (σ_H) for $SrGa_{0.75}Sc_{0.25}O_{2.5}$ calculated as the difference between the conductivity in H_2O-saturated argon (σ_{wet}) and the conductivity of the water-free sample (σ_{dry}).

The transference number for the proton conductivity (t_H) in wet argon can be calculated from the equation[17,20]

$$t_H = \frac{\sigma_H}{\sigma_{wet}}$$

The temperature dependence of t_H is given in Figure 13. The proton conductivity dominates in the low-temperature region, and a substantial decrease is observed only at $T > 623$ K.

Higher activation energies (E_A) are observed for the high-temperature part of the total conductivity in the heating cycle in dry argon and the cooling cycle in wet argon and in the whole temperature range for the cooling cycle in dry argon (Figure 11) in comparison with the low-temperature part (e.g., for the $SrGa_{0.75}Sc_{0.25}O_{2.5}$ sample cooled in wet argon, E_A = 1.21 eV at T = 873−1273 K, while at T = 573−773 K, it is only 0.71 eV). Such a high value of E_A at high temperature indicates predominant hole or oxide-ion conductivity. To reveal the nature of the high-temperature conductivity, conductivity

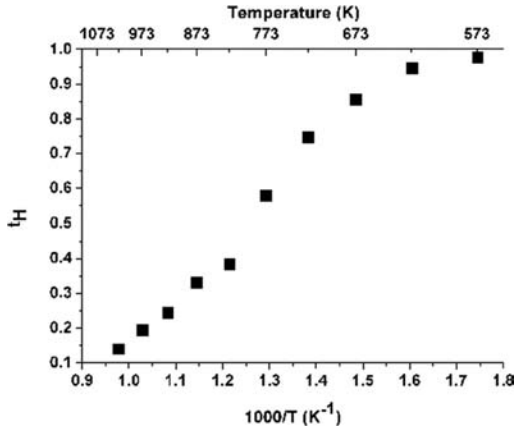

Figure 13. Proton-transfer number (t_H) in wet argon for $SrGa_{0.75}Sc_{0.25}O_{2.5}$.

measurements were performed for $SrGa_{0.75}Sc_{0.25}O_{2.5}$ in dry oxygen and dry argon. The corresponding Arrhenius plots are given in Figure 3 in the Supporting Information. The conductivity of $SrGa_{0.75}Sc_{0.25}O_{2.5}$ in dry oxygen is similar to that in dry argon, indicating a predominance of the oxide-ion conductivity in this compound under these conditions. Moreover, taking into account the total conductivity values at high temperature (8.5×10^{-3} S/cm at 1273 K) and expectedly low electronic conductivity for such types of oxides, one can propose moderate oxide-ion conductivity for $SrGa_{0.75}Sc_{0.25}O_{2.5}$.

4. DISCUSSION

The $A_2(B,B')_2O_5$ oxygen-deficient perovskites with only one type of A cation crystallize in different structure types, depending on the stable coordination number of the B cation. One type comprises oxides with Jahn−Teller B cations such as $Ca_2Mn_2O_5$,[21] $Sr_2Mn_2O_5$,[22−25] and $La_2Cu_2O_5$.[26] In their crystal structures, BO_5 square pyramids are connected by vertexes, forming a 3D framework (Figure 14a). In the crystal structure

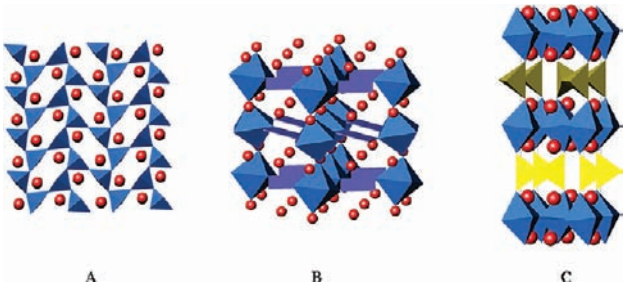

Figure 14. Crystal structures of different oxygen-deficient perovskites $A_2B_2O_5$: (a) $Sr_2Mn_2O_5$; (b) $La_2Ni_2O_5$; (c) brownmillerite $Ca_2(Fe,Al)_2O_5$.

of $La_2Ni_2O_5$, Ni^{2+} ($3d^8$) cations are distributed over an equal amount of corner-shared squares and octahedra (Figure 14b).[27,28] The brownmillerite structure type ($Ca_2(Fe,Al)_2O_5$) is the most widely spread among the $A_2(B,B')_2O_5$ compounds. It contains layers of corner-shared octahedra alternating with tetrahedral layers (Figure 14c). Brownmillerites with a single type of B cation or with several B cations are known. In the former case, the B cation should be stable in both tetrahedral and octahedral environments like in the case of $Sr_2Fe_2O_5$,[29] $Ca_2Fe_2O_5$,[30] $Ba_2In_2O_5$,[31] or $Sr_2In_2O_5$.[32] When different B cations are present, they can be fully or partially ordered over the octahedral and

dx.doi.org/10.1021/ic202236h | Inorg. Chem. 2012, 51, 1094−1103

tetrahedral positions in the brownmillerite structure for geometrical and/or electronic reasons. Full ordering is usually observed in compounds with Jahn−Teller cations, for example, in $LaSrCuGaO_5$[33] and M_2GaMnO_5, where M = Ca, Sr.[34,35] Partial ordering of B cations can be found in $Ca_2Ga(Al)FeO_5$[36,37] or $Sr(Ca)_2(Co,Ga)_2O_5$,[38,39] where the 3d metal cations preferentially occupy octahedral positions. In the above-listed structures, all corners of the BO_x polyhedra are connected with each other. To our knowledge, however, there is at least one example of the anion-deficient perovskite $Ba_3RM_2O_{7.5}$ (or $Ba_2R_{2/3}M_{4/3}O_5$, where R = rare-earth elements and M = Al, Ga)[40] in which structures there are tetrahedral units with some vertexes not connected to other B cations.

The studied $SrGa_{1-x}Sc_xO_{2.5}$ system provides a rare example of a variation of the B/B′ cation ratio with fixed oxygen content, leading to three different perovskite-related phases. The basis for such a behavior is a substantial difference in the size of Sc^{3+} and Ga^{3+} [$r(Sc^{3+}) = 0.73$ Å; $r(Ga^{3+}) = 0.62$ Å for CN = 6, and $r(Ga^{3+}) = 0.47$ Å for CN = 4[13]] and a strong preference of Sc^{3+} for an octahedral environment. As a consequence, variation of the Sc/Ga ratio in $SrGa_{1-x}Sc_xO_{2.5}$ is equivalent to variation of the octahedra/tetrahedra ratio. In Sr_2GaScO_5 ($x = 0.5$) with the brownmillerite structure, the octahedra and tetrahedra are present in equal amounts; thus, oxide represents an example of the structure in which a complete ordering of the B cations occurs mainly because of coupling with the ordering of the oxygen vacancies.

One can imagine several ways of transforming an ordered brownmillerite phase into a disordered cubic perovskite phase. The first one includes a temperature-induced phase transformation. An example of such a transformation is $Ba_2In_2O_5$ with the brownmillerite structure, which reversibly transforms to a disordered perovskite phase at $T > 930$ °C due to a disorder in the oxygen sublattice. The ordering of Ga^{3+} and Sc^{3+} in Sr_2GaScO_5 brownmillerite prevents a disorder of the oxygen vacancies without a disorder in the B cation sublattice. A complete disorder at both sublattices was achieved only by quenching the melt of this compound. Another common way to introduce disorder in the oxygen sublattice is an increase of the oxygen content in tetrahedral layers by the heterovalent substitution of A and/or B cations. This was done for Sr_2GaScO_5 by partial replacement of Sc^{3+} by Zr^{4+} according to the formula $SrGa_{0.5}Sc_{0.5-x}Zr_xO_{2.5+x/2}$. For Sr_2GaScO_5, a third way to transform to the cubic phase is the partial replacement of octahedral Sc^{3+} by Ga^{3+}, as achieved in the cubic perovskite $SrGa_{0.75}Sc_{0.25}O_{2.5}$. The substitution introduces disorder in the octahedral layers of the brownmillerite structure because of the substantial size difference between Ga^{3+} and Sc^{3+} cations and also allows disorder in the oxygen sublattice because Ga^{3+}, in comparison with Sc^{3+}, has a rather high flexibility of its coordination environment.

The transformation of the Sr_2GaScO_5 brownmillerite to a cubic perovskite by substitution of Sc^{3+} by Ga^{3+} does not occur continuously, and at intermediate composition, the novel $Sr_{10}Ga_6Sc_4O_{25}$ compound with a previously unknown type of ordering of B cations and O anions was isolated. Despite the resemblance of the lattice metrics and space group ($a = b \approx 2\sqrt{5}a_p$ and $c \approx 8a_p$; S.G. $I4_1/a$) to some elpasolite-type compounds like α-K_3AlF_6,[41] the crystal structure is different. In elpasolites, $A_2BB'F_6$, the B and B′ cations are ordered in a chessboard manner because of the substantial size and charge difference. Moreover, because one of the B cations represents a large alkaline cation, which prefers coordination numbers >6, sometimes large displacements of the anions take place. This leads to an increase of the coordination numbers of alkaline cations to CN = 7 and 8, like, e.g., in α-K_3AlF_6. In the crystal structure of $Sr_{10}Ga_6Sc_4O_{25}$, there is a complete ordering of B cations over the octahedral (Sc^{3+}) and tetrahedral (Ga^{3+}) sites. In comparison with brownmillerite Sr_2GaScO_5, the number of tetrahedra in $Sr_{10}Ga_6Sc_4O_{25}$ exceeds the number of octahedra by 50%. The oxygen stoichiometry $O_{2.5}$ is maintained by the fact that one-third of the tetrahedra in the $Sr_{10}Ga_6Sc_4O_{25}$ crystal structure have one vertex not connected with other Sc/Ga cations. A similar effect is also observed in the already mentioned $Ba_3RM_2O_{7.5}$ (or $Ba_2R_{2/3}M_{4/3}O_5$, where R = rare-earth elements and M = Al, Ga) anion-deficient perovskites.[40] In $Ba_3RM_2O_7$, the R^{3+} and M^{3+} cations, substantially different in size, are fully ordered over octahedral and tetrahedral sites. However, the arrangement of these polyhedra in $Ba_3RM_2O_{7.5}$ is completely different in comparison with that of $Sr_{10}Ga_6Sc_4O_{25}$.

Scandium-containing oxygen-deficient perovskites are known to exhibit proton conductivity because of the partial filling of the oxygen vacancies by water molecules and the formation of the hydroxyl groups according to the equation

$$H_2O + V_O^{\bullet\bullet} + O_O^{\times} \rightarrow 2OH_O^{\bullet}$$

Thus, $La_{0.6}Ba_{0.4}ScO_{2.8}$ exhibits high proton conductivity $\sim 1.5 \times 10^{-4}$ S/cm at 673 K.[42] We have shown that $SrGa_{0.75}Sc_{0.25}O_{2.5}$ is capable of conducting protons. However, its proton conductivity is much lower ($\sim 2.0 \times 10^{-6}$ S/cm at 673 K) in comparison with that of the doped $LaScO_3$. One can explain it by a high concentration of the remaining oxygen vacancies in the studied $SrGa_{0.75}Sc_{0.25}O_{2.5}$ samples, which are not filled by OH groups.

5. CONCLUSIONS

The $SrGa_{1-x}Sc_xO_{2.5}$ system provides a unique example of the substantial difference in the crystal chemistry of Sc^{3+} and Ga^{3+} cations, for which variation of the Sc/Ga ratio leads to three different perovskite-related phases with fixed oxygen content. In brownmillerite-like Sr_2GaScO_5, Sc^{3+} and Ga^{3+} cations are fully ordered over an equal amount of the octahedral and tetrahedral positions of the crystal structure. Partial substitution of scandium by gallium leads to the formation of $Sr_{10}Ga_6Sc_4O_{25}$ having a perovskite-like structure with a large unit cell ($a = b \approx 2\sqrt{5}a_p$ and $c \approx 8a_p$, where a_p = perovskite subcell parameter). Like in the case of brownmillerite, in its structure, a full ordering of Ga^{3+} and Sc^{3+} over tetrahedral and octahedral positions takes place. However, the number of tetrahedral positions in $Sr_{10}Ga_6Sc_4O_{25}$ is by 50% higher in comparison with the number of octahedral ones. This leads to the fact that one-third of the tetrahedra have one vertex not connected with other Sc/Ga cations. Further substitution of Sc^{3+} by Ga^{3+} leads to the complete disorder of the B cations and oxygen vacancies and to the formation of $SrGa_{0.75}Sc_{0.25}O_{2.5}$ with the cubic perovskite structure. This compound is capable, as are other scandium-containing perovskites, of being a proton conductor with $\sigma_H = 2.0 \times 10^{-6}$ S/cm at 673 K.

■ ASSOCIATED CONTENT

Ⓢ Supporting Information

Table of final atomic coordinates and displacement parameters for $Sr_{10}Ga_6Sc_4O_{25}$, X-ray crystallographic files of the refined structures in CIF format, and additional figures. This material is available free of charge via the Internet at http://pubs.acs.org.

dx.doi.org/10.1021/ic202236h | Inorg. Chem. 2012, 51, 1094−1103

AUTHOR INFORMATION

Corresponding Author

*E-mail: istomin@icr.chem.msu.ru. Tel.: +7 495 9393490. Fax: +7 495 9394788.

Author Contributions

All authors have given approval to the final version of the manuscript.

ACKNOWLEDGMENTS

This work was partially supported by RFBR (Grant 11-03-01225) and by the Swedish Research Council and Swedish Institute (Visbyprogramme). The authors gratefully acknowledge Professor A. V. Shevelkov (Moscow State University) for valuable discussions.

REFERENCES

(1) Malavasi, L.; Fisher, C. A. J.; Islam, M. S. *Chem. Soc. Rev.* **2010**, *39*, 4370−4387.
(2) Ishihara, T.; Matsuda, H.; Takita, Y. *J. Am. Chem. Soc.* **1994**, *116*, 3801−3803.
(3) Feng, M.; Goodenough, J. *Eur. J. Solid State Inorg. Chem.* **1994**, *31*, 663−672.
(4) Goodenough, J.; Ruez-Diaz, J.; Zhen, Y. *Solid State Ionics* **1990**, *44*, 21−31.
(5) Kakinuma, K.; Yamamura, H.; Haneda, H.; Atake, T. *Solid State Ionics* **2002**, *154*− *155*, 571−576.
(6) Antipov, E. V.; Shpanchenko, R. V.; Lykova, L. N.; Kovba, L. M. *Kristallografiya* **1990**, *35*, 213.
(7) Antipov, E. V.; Lykova, L. N.; Kovba, L. M. *Sov. J. Coord. Chem.* **1985**, *11*, 1151.
(8) Rath, M.; Müller-Buschbaum, Hk. *J. Alloys Compd.* **1992**, *189*, 127−130.
(9) Takeda, Y.; Imanishi, N.; Kanno, R.; Mizuno, T.; Higuchi, H.; Yamamoto, O.; Takano, M. *Solid State Ionics* **1992**, *53*−*56*, 748−753.
(10) Douy, A. *Int. J. Inorg. Mater.* **2001**, *3*, 699−707.
(11) Larson, A. C.; Von Dreele, R. B. General Structure Analysis System (GSAS). *Los Alamos National Laboratory Report LAUR*; Los Alamos National Laboratory: Los Alamos, NM, 2000; pp 86−748.
(12) Lindberg, F.; Svensson, G.; Istomin, S. Ya.; Aleshinskaya, S. V.; Antipov, E. V. *J. Solid State Chem.* **2004**, *177*, 1592−1597.
(13) Shannon, R. D.; Prewitt, C. T. *Acta Crystallogr.* **1969**, *B25*, 925−946.
(14) Favre-Nicolin, V.; Cerny, R. *J. Appl. Crystallogr.* **2002**, *35*, 734−743.
(15) Kobzareva, V. P.; Kovba, L. M.; Lopato, L. M.; Lykova, L. N.; Shevchenko, A. V. *Russ. J. Inorg. Chem.* **1976**, *21*, 903−904.
(16) Fujii, H.; Katayama, Y.; Shimura, T.; Iwahara, H. *J. Electroceram.* **1998**, *2*, 119−125.
(17) Lybye, D.; Bonanos, N. *Solid State Ionics* **1999**, *125*, 339−344.
(18) Nomura, K.; Takeuchi, T.; Kamo, S.; Kageyama, H.; Miyazaki, Y. *Solid State Ionics* **2004**, *175*, 553−555.
(19) Zhang, G. B.; Smyth, D. M. *Solid State Ionics* **1995**, *82*, 153−160.
(20) Kato, H.; Yugami, H. *J. Electroceram.* **2007**, *18*, 219−224.
(21) Poeppelmeier, K. R.; Leonowicz, M. E.; Scanlon, J. C.; Longo, J. M.; Yelon, W. B. *J. Solid State Chem.* **1982**, *45*, 71−79.
(22) Caignaert, V.; Nguyen, N.; Hervieu, M.; Raveau, B. *Mater. Res. Bull.* **1985**, *20*, 479−484.
(23) Caignaert, V. *J. Magn. Magn. Mater.* **1997**, *166*, 117−123.
(24) Mori, T.; Inoue, K.; Kamegashira, N.; Yamaguchi, Y.; Ohoyama, K. *J. Alloys Compd.* **2000**, *296*, 92−97.
(25) Suescun, L.; Chmaissem, O.; Mais, J.; Dabrowski, B.; Jorgensen, J. D. *J. Solid State Chem.* **2007**, *180*, 1698−1707.
(26) Khasanova, N. R.; Izumi, F.; Hiroi, Z.; Takano, M.; Huang, Q.; Santoro, A. *Acta Crystallogr.* **1996**, *C52*, 2381−2384.
(27) Alonso, J. A.; Martinez-Lope, M. J. *J. Chem. Soc., Dalton Trans.* **1995**, *17*, 2819−2824.
(28) Alonso, J. A.; Martinez-Lope, M. J.; Garcia-Munoz, J. L.; Fernandez, M. T. *Physica B* **1997**, *234*−*236*, 18−19.
(29) Greaves, C.; Jacobson, A. J.; Tofield, B. C.; Fender, B. E. F. *Acta Crystallogr.* **1975**, *B31*, 641−646.
(30) Bertaut, F.; Blum, P.; Sagnieres, A. *C. R. Acad. Sci.* **1957**, *244*, 2944−2946.
(31) Gregory, D. H.; Weller, M. T. *J. Solid State Chem.* **1993**, *107*, 134−148.
(32) von Schenk, R.; Müller-Buschbaum, H. *Z. Anorg. Allg. Chem.* **1973**, *395*, 280−286; *Z. Anorg. Allg. Chem.* **1974**, *405*, 200−200.
(33) Vaughey, J. T.; Wiley, J. B.; Poeppelmeier, K. R. *Z. Anorg. Allg. Chem.* **1991**, *598*, 327−338.
(34) Abakumov, A. M.; Rozova, M. G.; Pavlyuk, B. P.; Lobanov, M. V.; Antipov, E. V.; Lebedev, O. I.; van Tendeloo, G.; Ignatchik, O. L.; Ovtchenkov, E. A.; Koksharov, Yu. A.; Vasil'ev, A. N. *J. Solid State Chem.* **2001**, *160*, 353−361.
(35) Abakumov, A. M.; Rozova, M. G.; Pavlyuk, B. P.; Lobanov, M. V.; Antipov, E. V.; Lebedev, O. I.; van Tendeloo, G.; Sheptyakov, D. V.; Balagurov, A. M.; Bouree, F. *J. Solid State Chem.* **2001**, *158*, 100−111.
(36) Bertaut, E. F.; Blum, P.; Sagnieres, A. *Acta Crystallogr.* **1959**, *12*, 149−159.
(37) Arpe, R.; von Schenk, R.; Müller-Buschbaum, H. *Z. Anorg. Allg. Chem.* **1974**, *410*, 97−103.
(38) Lindberg, F.; Istomin, S. Ya.; Berastegui, P.; Svensson, G.; Kazakov, S. M.; Antipov, E. V. *J. Solid State Chem.* **2003**, *173*, 395−406.
(39) Istomin, S. Ya.; Abdyusheva, S. V.; Svensson, G.; Antipov, E. V. *J. Solid State Chem.* **2004**, *177*, 4251−4257.
(40) Abakumov, A. M.; Shpanchenko, R. V.; Lebedev, O. I.; Van Tendeloo, G.; Amelinckx, S.; Antipov, E. V. *Acta Crystallogr.* **1999**, *A55*, 828−839.
(41) Abakumov, A. M.; King, G.; Laurinavichute, V. K.; Rozova, M. G.; Woodward, P. M.; Antipov, E. V. *Inorg. Chem.* **2009**, *48*, 9336−9344.
(42) Kim, S.; Lee, K. H.; Lee, H. L. *Solid State Ionics* **2001**, *144*, 109−115.